Ceramics International 51 (2025) 28460–28466

Contents lists available at ScienceDirect

Ceramics International

journal homepage: www.elsevier.com/locate/ceramint

Short communication

Effect of lattice strain on stabilization temperature of calcium added (Mg, Co, Ni, Cu, Zn)O

Ashwani Gautam, Md Imteyaz Ahmad *

Department of Ceramic Engineering, Indian Institute of Technology (BHU), Varanasi, 221005, India

ARTICLE INFO

Handling Editor: Dr P. Vincenzini

Keywords:
High entropy oxides
Multicomponent oxides
Isovalent substitution
Lattice strain energy

ABSTRACT

The effect of lattice strain due to relatively larger isovalent cation substitution on the stability landscape of equiatomic (Mg, Co, Ni, Cu, Zn)O high entropy oxide is explored. A simple yet effective formulation to incorporate strain energy for calculating critical temperature for high entropy single-phase rocksalt phase formation is proposed. The estimated phase stabilization temperature is successfully validated for varying substitution calcium (x = 0.05, 0.1, 0.16) in $(Co, Mg, Ni, Cu, Zn)_{1-x}Ca_xO$. We used XRD and electron microscopy to confirm the single-phase formation of rocksalt HEOs.

1. Introduction

The concept of the mixing of multiple principal components (element/compound) in nearly equimolar concentrations has resulted in several new compositions with novel properties. Cantor and Yeh were the first to demonstrate the synthesis of an equimolar multi-element single-phase alloy [1,2]. Although several names of this material class were proposed such as multi-component alloys, and multi-principal element alloys. Later, this class of material was designated as high entropy alloys (HEAs) [1–3]. The discovery of high entropy alloys has sparked a lot of attention as it opened up the prospect of using high configurational entropies (≥1.609R per mole of an atom) to stabilize a phase [4]. The concept of entropic stabilization has recently been expanded to the oxide system and named high entropy oxides (HEOs) [5–7]. Owing to the high configuration entropy of mixing, HEO tends to stabilize a single phase solid solution such as rocksalt [5], spinel [8], fluorite [9], and perovskite. Hume-Rothery and Paulling's principles dictate the basic rationale for the selection of components for the formation of a single-phase solid solution, which includes similar ionic radii and the same oxidation state for the specific lattice structure [10]. Using these criteria, the simple MO rocksalt structure (M = Mg, Ni, Co, Zn, Cu) was first synthesized by Rost et al., in 2015 [3]. It has been established that entropic contribution to the Gibbs free energy may be exploited to stabilize the new oxide phase. It was initially suggested that an increase in ΔS_{mix} of an equiatomic multi-element alloy might favour the single-phase formation over competing intermetallic phases; however, experiments revealed that in many cases configuration entropy could not overcome the contrasting driving force, i.e. enthalpy. Therefore, a high entropy does not guarantee the formation of a single-phase solid solution. For the stabilization of a single-solid solution, TΔS should be enough to compensate for the positive enthalpy term. [12]. Incorporating six components could theoretically boost the configurational entropy, enhancing single-phase stabilization. However, this benefit is contingent upon avoiding microstates, any kind of ordering effects, or defect proliferation that might lower the enthalpy [11]. Additionally, maintaining structural electroneutrality, whether through accommodating larger cations or creating vacancies, must remain energetically viable [12,13]. Since each ion in a perfect crystal occupies a specific symmetry site within the unit cell, if the substitutional ion has the size and charge comparable to the ion it replaces, then it can occupy lattice positions with little disruption. The size difference between the host ion and substitutional ion causes strain in the lattice; as a result, ions in the crystal lattice shift their position until all the neighbouring ions experience zero force [14]. Increasing interest in the synergistic effects on properties in HEOs has been a driving force for designing and examining systems with five or more components. This effort has been tremendously useful to the materials community since it has resulted in the development of several novel systems with specific properties [15–18]. There are several studies indicating that the addition of cations of varying sizes changes the stabilization temperature of the high entropy phase. For instance, Chen et al. [19] demonstrated that the stabilization temperature of rocksalt medium entropy oxides

* Corresponding author.
E-mail address: imteyazahmad.cer@iitbhu.ac.in (M.I. Ahmad).

https://doi.org/10.1016/j.ceramint.2025.03.449
Received 31 December 2024; Received in revised form 15 March 2025; Accepted 30 March 2025
Available online 1 April 2025

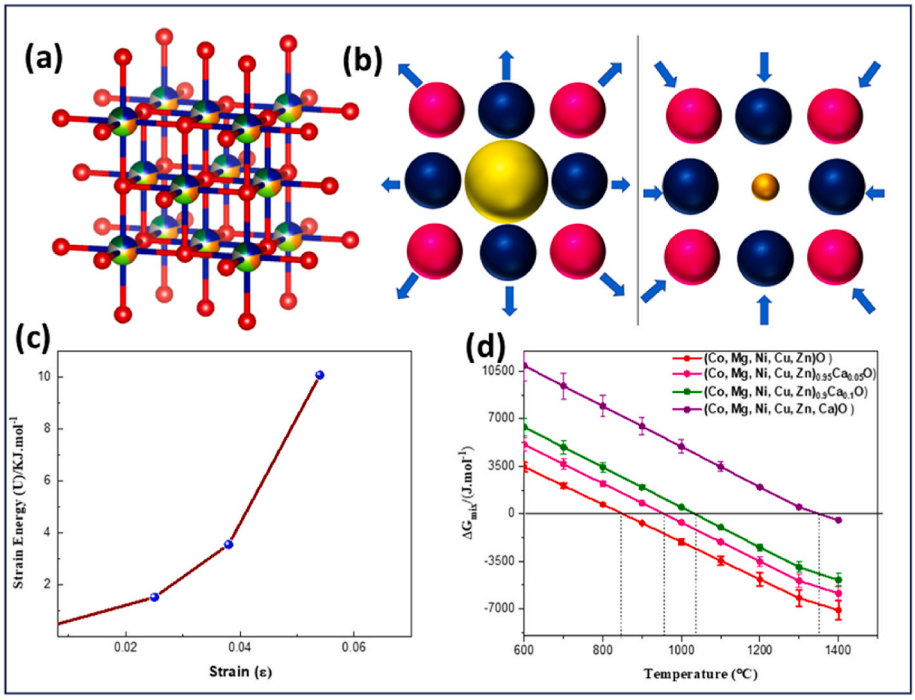

Fig. 1. (a) Schematic showing the rocksalt crystal structure of HEO, (b) stress-induced in the lattice due to substitution of cation (yellow) with larger ionic radius (*a*) and with smaller ionic radii on host oxide system. Here blue and red spheres represent cation and oxygen as anions, respectively. (c) plot depicts the relationship between Gibbs free energy and temperature for the synthesis of single phase rocksalt structure (b) the relationship between strain energy vs strain due to ionic size mismatch. (For interpretation of the references to colour in this figure legend, the reader is referred to the Web version of this article.)

Table 1
The estimated strain, strain energy, enthalpy, entropy and critical temperature for single-phase formation.

Sample	ε	U (kJ/mol)	ΔH (kJ/mol)	ΔS (J/k-mol)	T_C (°C)
Parent HEO	0	0	15	13.38	848
x = 0.05	0.025	1.74	17.66	14.35	957
x = 0.1	0.038	3.97	19.35	14.70	1043
x = 0.16	0.064	10.94	24.27	14.87	1359

increased linearly with the substitution of Zn^{2+}. Anand et al. [20] investigated the role of configurational entropy and estimated thermodynamic properties of various oxide mixes and elucidated that the enthalpy penalty reduces with the number of cations making it easier to stabilize. However, no systematic study has been undertaken to quantify the effect of strain due to the addition of cations of varying radii on the phase stability of high entropy oxides. In the present work, Ca^{2+} having significantly different ionic radii is substituted in the equiatomic quinary (Co, Mg, Ni, Cu, Zn)O to synthesize single phase (Co, Mg, Ni, Cu, $Zn)_{1-x}Ca_xO$ (x = 0.05, 0.1, 0.16) HEO using solution combustion synthesis (SCS) route [13,21–24]. A simple model is utilized to quantify the strain and its effect on overall enthalpy and the stabilization temperature.

2. Experimental

We used SCS to synthesize HEO nanocrystalline powder using metal nitrate precursor including Cobalt (II) nitrate hexahydrate Co $(NO_3)_2$•$6H_2O$, copper nitrate trihydrate $Cu(NO_3)_2$•$3H_2O$, nickel nitrate hexahydrate $Ni(NO_3)_2$•$6H_2O$, magnesium nitrate hexahydrate Mg(NO3) 2•$6H_2O$, zinc nitrate hexahydrate Zn(NO3)2•6H2O, calcium nitrate tetrahydrate $Ca(NO_3)_2.4H_2O$ were purchased from the Merk (purity assay~ 99 %). All reagents were of analytical grade and used as received without further purification. A 0.2 M solution of each metal nitrate precursor was dissolved in 40 ml of distilled water, followed by mixing of an appropriate amount of citric acid ($C_6H_8O_7$) at room temperature using magnetic stirring. pH of the solution was adjusted using 30 % ammonia solution. The solution formed was stirred continuously for 24

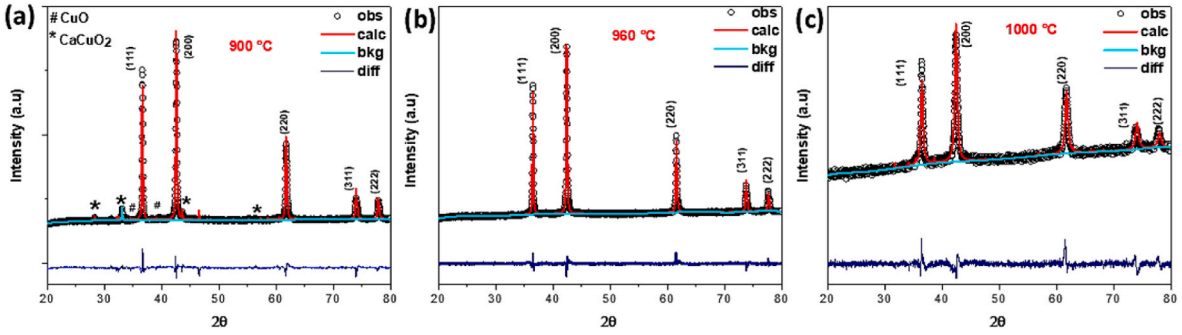

Fig. 2. XRD pattern depicting phase evolution of TM-HEO5 powder sample at a temperature (a) 900 °C and (b) 960 °C (c) 1000 °C respectively. Phase pure rocksalt structure obtained on annealing at temperatures ≥960 °C (T_C).

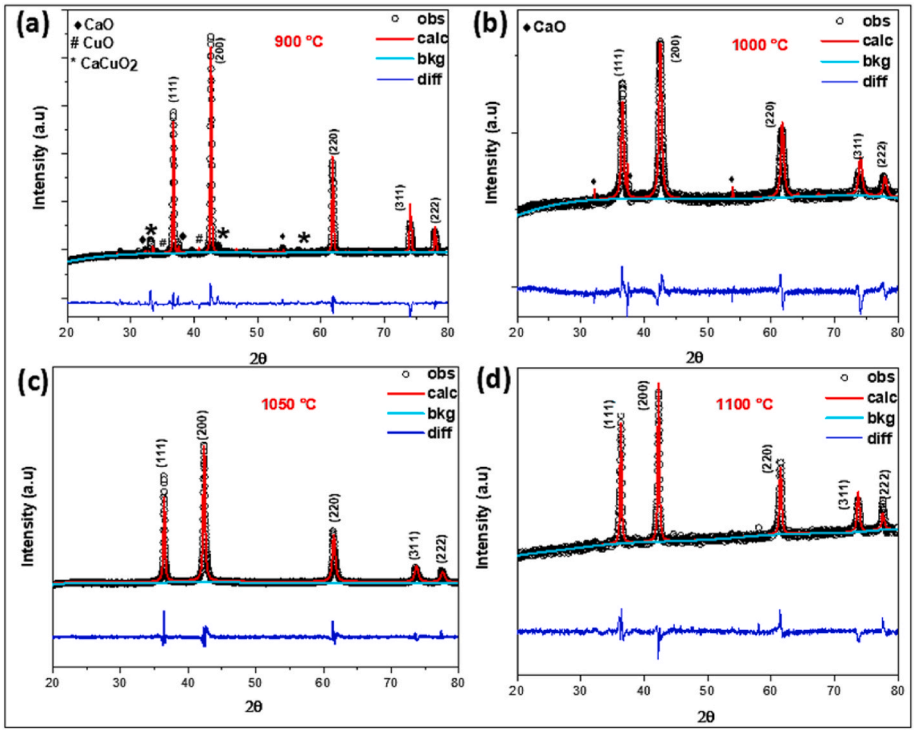

Fig. 3. XRD spectra revealing phase evolution of TM-HEO10 powder sample at temperature (a) 900 °C (b)1000 °C (c) 1050 °C (d) 1100 °C respectively. Phase pure rocksalt structure obtained at $T_C \geq 1050$ °C.

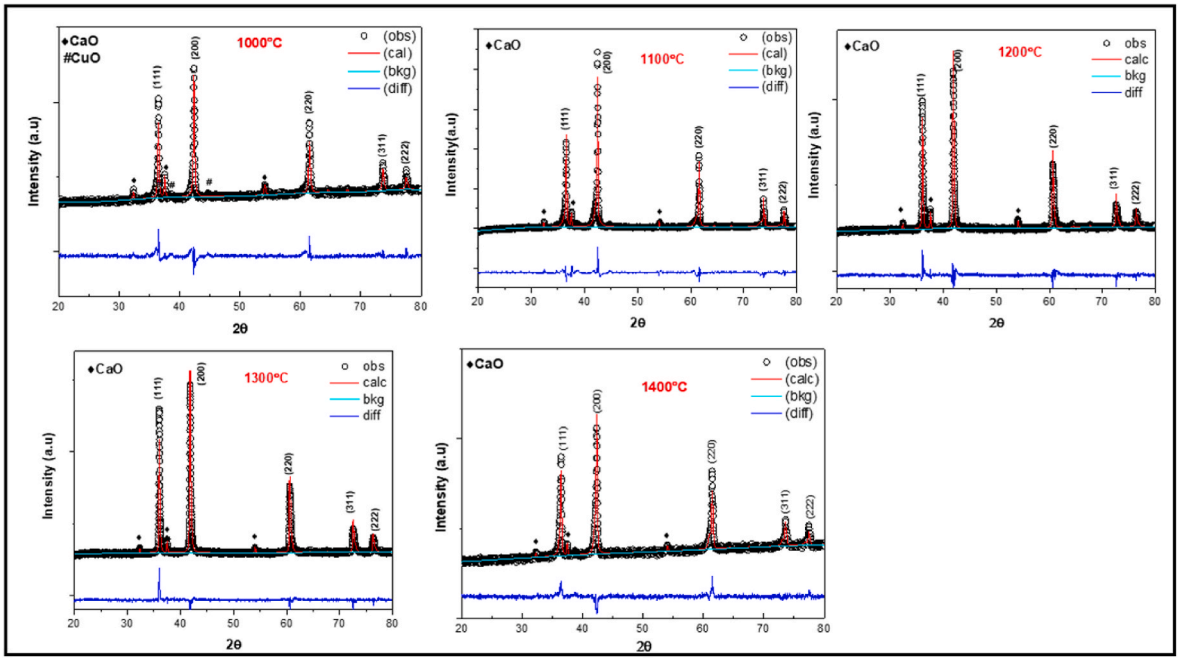

Fig. 4. XRD patterns of equiatomic (Co, Mg, Ni, Cu, Zn, Ca)O (TM-HEO16) powder annealed at varying temperatures from 1000 °C to 1400 °C.

h at 80 °C using a magnetic stirrer which resulted in the formation of dark blue gel. Thereafter, the temperature was increased slowly to the range of 300–350 °C until the combustion reaction was ignited, resulting nanocrystalline fluffy powers. The resulting fluffy powders were then calcined at 900°C–1400 °C to achieve $(Co, Mg, Ni, Cu, Zn)_{0.2}O$, and $(Co, Mg, Ni, Cu, Zn)_{1-x}Ca_xO$ (x = 0.05, 0.1, 0.16) HEO powders (hereafter indicated as TM-HEO0, TM-HEO5, TM-HEO10 and TM-HEO16, respectively). The crystallographic phase analysis of the nanocrystalline powders was performed using an X-ray diffractometer (Rigaku Mini-flex 600) operating at 40 kV and 15 mA with Cu-Kα radiation (λ = 0.154 nm). XRD patterns were recorded over a 2θ range of 20°–80° at a scan rate of 2°/min and a step size of 0.02°. Rietveld refinement of XRD patterns was done using GSAS2 software suit. The elemental mapping and composition quantification of the calcined powders were analyzed using a scanning electron microscope (SEM, Nova Nano 450) equipped with energy-dispersive X-ray spectroscopy (EDS). Phase purity and

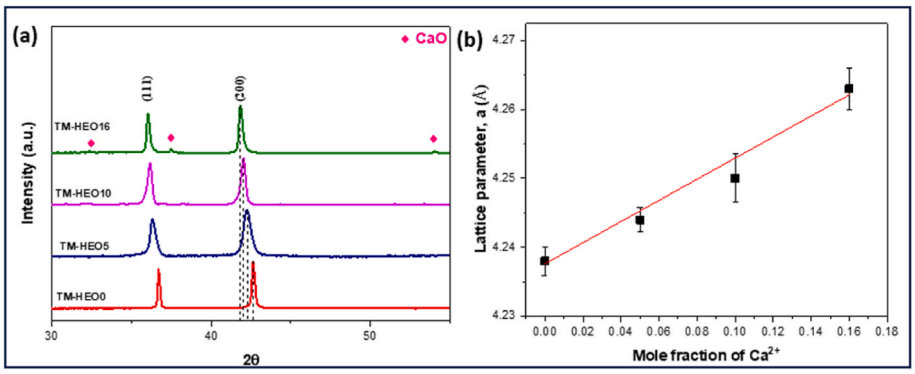

Fig. 5. XRD patterns of powder sample of (a) five components HEO (TM-HEO0) and Ca added (Co, Mg, Ni, Cu, Zn)$_{1-x}$Ca$_x$O HEO at different compositions (x = 0.05,0.10 and 0.16) at 900 °C,1000 °C,1100 °C and 1400 °C, respectively; (b) depicts the increase in lattice parameter as fraction of mole fraction of Ca^{2+}.

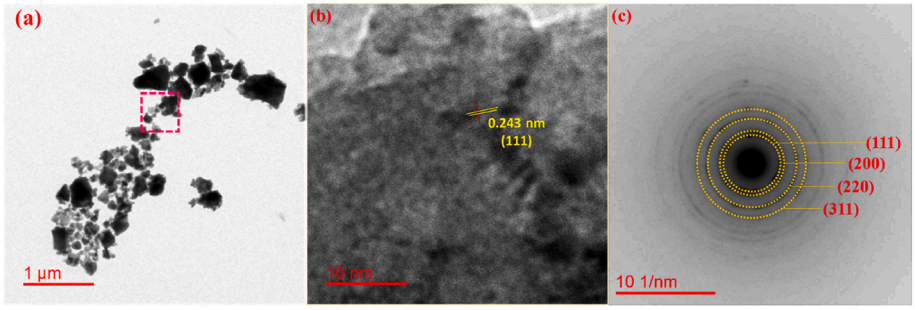

Fig. 6. (a) Bright-field TEM image (b) phase contrast image showing interplanar distance 0.243 nm and (c) SAED pattern showing polycrystalline nature of TM-HEO0 sample.

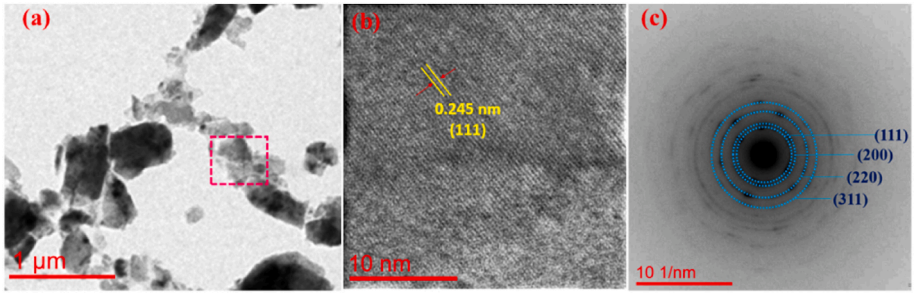

Fig. 7. (a) Bright-field TEM image (b) phase contrast image showing inter-planar distance 0.245 nm and (c) SAED pattern showing polycrystalline nature of TM-HEO5 sample.

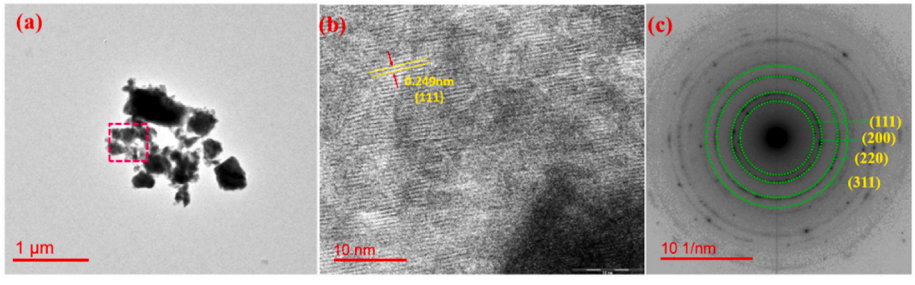

Fig. 8. (a) Bright-field TEM image, (b) phase contrast image showing interplanar distance 0.249 nm, and (c) SAED pattern showing polycrystalline nature of TM-HEO10 sample.

crystallinity of the synthesized samples were analyzed by TEM (Tecnai G2 20 TWIN, FEI) under an operating voltage of 200 kV. Samples for TEM imaging were prepared by dispersing the powder in ethanol through ultrasonication for 90 min followed by drop-casting on a 200-mesh carbon-coated Cu grid.

3. Results and discussion

The strain due to the large ionic size of the Ca^{2+} doping in (Co, Mg, Ni, Cu, Zn)O has been shown to influence the formation of single-phase and change the phase stability landscape [20,25,26]. The strain ε due to a larger cation (Ca^{2+}) substitution is described by Ref. [27]:

$$\varepsilon = \frac{\partial r}{r} \tag{1}$$

$$\varepsilon = \frac{\overline{r}_1 - \overline{r}_0}{\overline{r}_0} \tag{2}$$

where $\overline{r}_0, and\, \overline{r}_1$ are the average ionic radii of the parent HEO cations and Ca^{2+} substituted six component HEO, respectively. The effective radius of Ca^{2+} substituted HEO at different doping concentrations is calculated by using the relation [28].

$$\overline{r}_1 = \sum_{i=1}^{6} (n_i \,.r_i\,) \tag{3}$$

where $n_i\,, r_i$ is the molar concentration of constituent cations and their ionic radius. Fig. 1(a) shows the schematic of the crystal structure of rocksalt five component HEO. Since in rock-salt structure, cation and anion are arranged in a cubic lattice, volumetric strain is determined by the relation

$$\varepsilon_v = \frac{\partial V}{V} = 3\frac{\partial a}{a} \tag{4}$$

$$\varepsilon_v = \frac{3(a_{sub} - a_{par})}{a_{par}} \tag{5}$$

where a_{sub}, and a_{par} are the lattice parameters of Ca^{2+} substituted HEO and the parent TM-HEO0, respectively. For equation (4), it was assumed that the lattice experiences the hydrostatic state of strain. Fig. 1(b) shows how ionic size mismatch creates local strain in the lattice. For estimating strain energy stored in the lattice due to the substitution of larger size Ca^{2+} into the lattice of the five-element HEOs, it was assumed that TM-HEO0 experiencing negligible strain (as ionic radii of the TM cations are nearly the same; 0.69–0.72 Å) and taken as reference. The strain energy equivalent to local elastic pressure for the structural decomposition was calculated from the lattice strain model proposed by Brice et al., [27,29–31]

$$U = 4\pi E N_A \left(\frac{\overline{r}_0}{2}(\overline{r}1 - \overline{r}0)^2 + \frac{1}{3}(\overline{r}1 - \overline{r}0)^3 \right) \tag{6}$$

where U is the strain energy in $kJmol^{-1}$, E is Young's modulus of the HEO (108 GPa [32]). $\overline{r}_0, and\, \overline{r}_1$ are the average ionic radii of cations in five-component TM-HEO0 and Ca^{2+} added six-component HEOs, respectively. Fig. 1(c) depicts a plot of strain energy due to large-size cation substitution. This strain energy was added to the enthalpy of mixing (ΔH) to calculate the critical temperature beyond which ΔG become negative for the single-phase formation [33]. Thus, it was evaluated that strain energy on increasing Ca^{2+} concentration enhanced the enthalpy of mixing. In addition to the strain effect, the enthalpy penalty (ΔH) for $(Co, Mg, Ni, Cu, Zn)_{1-x}Ca_xO$ (x = 0.05, 0.1, 0.16) system involves enthalpy change associated with the phase transition of ZnO (wurtzite to rocksalt) and CuO (tenorite to rocksalt). The enthalpy associated with the phase transition to rocksalt for ZnO and CuO was reported 25 $kJmol^{-1}$ and 22 $kJmol^{-1}$, respectively [5,32]. The crystal structure of CaO (sixth constituent) is also the same with some marginal difference in lattice parameter (4.80 Å) from the final states (4.23 Å). There is only a volume misfit in the case of CaO and thus doesn't involve a significant enthalpy change associated with the structural transition. For simplicity, we assumed that the solution of each binary oxide into rocksalt is ideal. To account for the structural transition of ZnO and CuO, enthalpic penalties were calculated based on a product of the mole fractions of each component multiplied by reference transition enthalpy, including the strain effect. Thus, the overall driving force (ΔH) can be formulated as:

$$\Delta H = U_{Ca^{2+}} + x_i(25\,) + y_i(22)\ \mathrm{kJ{\cdot}mol^{-1}} \tag{7}$$

where x_i, and y_i represents the molar compositions of ZnO and CuO, respectively. The configurational entropy of parent equiatomic HEO (Co, Mg, Ni, Cu, Zn)O and Ca^{2+} added HEOs are calculated using the relation [34]:

$$\Delta S_{config.} = -\mathrm{R}\left(\sum_{i=1}^{n} x_i \ln x_i \right)_{cation} \tag{8}$$

Phase formation is governed by the minimization of Gibbs free energy which is connected to the enthalpy ΔH and entropy ΔS, through the equation [6,28].

$$\Delta G = \Delta H - T\Delta S \tag{9}$$

It is obvious that in the case ΔH > 0, the entropy term (TΔS) should be high enough to surpass the enthalpy penalty so that ΔG becomes negative for single-phase formation [6]. Since the configuration entropy for the random solid solution phase is constant, it can be stable above a critical temperature (T_c). Fig. 1 (d) shows variation in the estimated critical temperature for varying Ca^{2+} substitution. The estimated critical temperature increases with the calcium addition. The critical temperature increased from 848 °C for the parent HEO to 957, 1043, and 1359 °C for 0.05, 0.1 and 0.16 mol fraction Ca^{2+} substitution (Table 1). A similar observation was made by Chen et al., [19] for a four-component medium entropy oxide where stabilization temperature increased linearly with the substitution of Zn^{2+}. The increase in the critical stabilization temperature was due to the positive enthalpy associated with the wurtzite to rocksalt transition of ZnO.

To validate the estimated critical temperature, the five-component HEO (TM-HEO0) and Ca^{2+} substituted samples (TM-HEO5, TM-HEO10 and TM-HEO16) were synthesized by solution combustion methods and annealed to form a single phase. X-ray diffraction patterns were recorded after annealing at varying temperatures at intervals of 100 °C and analyzed to examine the phase and structural parameters ((Fig. 2(a–c) and Fig. 3(a–d)). For samples having x = 0.05 and x = 0.1 in $(Co, Mg, Ni, Cu, Zn)_{1-x}Ca_xO$, single-phase rock-salt (space group $Fm\bar{3}m$) is observed on annealing at temperatures 960, and 1050 °C, which is close to the calculated values of 957 and 1043 °C, respectively (Figs. 2 (b) and 3(c)). Below this critical temperature, in addition to the prominent rocksalt phase, some other phases are observed which could be indexed to the tenorite (CuO), wurtzite (ZnO), and traces of intermediate $CaCuO_2$ phase (Figs. 2a, 3a and 3b). The presence of separate phases was attributed to the greater positive enthalpy (ΔH) than to the negative TΔS term, below the critical temperature. On increasing the temperature above the estimated critical temperature, single phase solid solution was observed.

The estimated critical temperature for TM-HEO16 was 1359 °C; however, even after heating to 1400 °C, CaO peaks were observed, although the intensity of CaO peaks decreased significantly. XRD pattern of TM-HEO16 annealed at different temperatures is depicted in Fig. 4. For TM-HEO16, apart from prominent peaks belonging to the rocksalt phase, there are minor peaks of CaO (estimated to be ~4 mol% from Rietveld analysis) present even after annealing at 1400 °C. Since the difference in ionic radius of the calcium ion and the average size of the cation in the host (Co, Mg, Ni, Cu, Zn) O is 37.89 % which is much larger and can impose a solubility limit on Ca^{2+} in the parent HEO [11]. This indicates that the solubility limit of Ca^{2+} is somewhere between 0.1 and 0.12 mol fraction.

It is obvious from Fig. 5(a) that the diffraction peaks shift to lower angles on increasing Ca^{2+} concentration, indicating lattice parameter

increase, which is plotted in Fig. 5(b). The lattice parameter of the high entropy rocksalt phase was calculated from the XRD patterns. An increase in lattice parameters follows a linear trend with the Ca^{2+} content. This shows that the interaction parameter for Ca^{2+} substitution in the HEO is rather small if not zero. The elemental mapping of all the samples using SEM-EDS (Figs. S1–S4) confirms the random and uniform distribution of all constituent elements.

To confirm the phase purity and crystallinity of the synthesized samples, we performed TEM analysis at several spots. Representative images and SAED patterns are shown in Figs. 6–8 for TM-HEO0, TM-HEO5 and TM-HEO10, respectively. The bright field TEM image and corresponding phase contrast images (Figs. 6a, 7a and 8a) and SAED patterns (Figs. 6c, 7c and 8c) confirm the phase purity and crystallinity. SAED in all the cases could be indexed to the rocksalt phase. Figs. 6b, 7b and 8b show the lattice fringes with inter-planar distances of 0.243,0.245, and 0.249 nm in the phase contrast image is attributed to (111) planes of rocksalt phase of sample TM-HEO0, TM-HEO5 and TM-HEO10, respectively.

4. Conclusions

A formulation for accounting the strain energy for the dissolution of larger isovalent cation into high entropy phase formation is proposed and validated by substituting Ca^{2+} in (Mg, Co, Ni, Cu, Zn)O. The strain due to the large size of the Ca^{2+} caused a larger activation energy barrier, for the formation of single-phase rocksalt solid solution (Co, Mg, Ni, Cu, Zn)$_{1-x}$Ca$_x$O, which enhanced the critical temperature for entropic stabilization (TΔS). The critical temperature for single-phase solution phase formation increased from 875 °C for (Co, Mg, Ni, Cu, Zn) O to around 960 and 1050 °C for (Co, Mg, Ni, Cu, Zn)$_{0.95}$Ca$_{0.05}$O and (Co, Mg, Ni, Cu, Zn)$_{0.9}$Ca$_{0.1}$O. In the case of equimolar six-component (Co, Mg, Ni, Cu, Zn, Ca) O HEO, although the critical estimated temperature was 1359 °C, even after heating to 1400 °C only about 0.12 mol fraction of Ca^{2+} could be dissolved, indicating to the solubility limit imposed by the large cationic size difference.

CRediT authorship contribution statement

Ashwani Gautam: Writing – original draft, Validation, Methodology, Investigation, Conceptualization. **Md Imteyaz Ahmad:** Writing – review & editing, Supervision, Conceptualization.

Declaration of competing interest

The authors declare that they have no known competing financial interests or personal relationships that could have appeared to influence the work reported in this paper.

Appendix A. Supplementary data

Supplementary data to this article can be found online at https://doi.org/10.1016/j.ceramint.2025.03.449.

References

[1] B. Cantor, I.T.H. Chang, P. Knight, A.J.B. Vincent, Microstructural development in equiatomic multicomponent alloys, Mater. Sci. Eng. 375–377 (2004) 213–218, https://doi.org/10.1016/j.msea.2003.10.257.

[2] J.W. Yeh, S.K. Chen, S.J. Lin, J.Y. Gan, T.S. Chin, T.T. Shun, C.H. Tsau, S.Y. Chang, Nanostructured high-entropy alloys with multiple principal elements: novel alloy design concepts and outcomes, Adv. Eng. Mater. 6 (2004) 299–303, https://doi.org/10.1002/adem.200300567.

[3] D.B. Miracle, O.N. Senkov, A critical review of high entropy alloys and related concepts, Acta Mater. 122 (2017) 448–511, https://doi.org/10.1016/j.actamat.2016.08.081.

[4] S. Guo, C.T. Liu, Phase Stability in High Entropy Alloys: Formation of Solid-Solution Phase or Amorphous Phase, n.d.

[5] C.M. Rost, E. Sachet, T. Borman, A. Moballegh, E.C. Dickey, D. Hou, J.L. Jones, S. Curtarolo, J.P. Maria, Entropy-stabilized oxides, Nat. Commun. 6 (2015), https://doi.org/10.1038/ncomms9485.

[6] S.J. McCormack, A. Navrotsky, Thermodynamics of high entropy oxides, Acta Mater. 202 (2021) 1–21, https://doi.org/10.1016/j.actamat.2020.10.043.

[7] C. Oses, C. Toher, S. Curtarolo, High-entropy ceramics, Nat. Rev. Mater. 5 (2020) 295–309, https://doi.org/10.1038/s41578-019-0170-8.

[8] A. Mao, F. Quan, H.Z. Xiang, Z.G. Zhang, K. Kuramoto, A.L. Xia, Facile synthesis and ferrimagnetic property of spinel (CoCrFeMnNi)3O4 high-entropy oxide nanocrystalline powder, J. Mol. Struct. 1194 (2019) 11–18, https://doi.org/10.1016/j.molstruc.2019.05.073.

[9] J. Gild, M. Samiee, J.L. Braun, T. Harrington, H. Vega, P.E. Hopkins, K. Vecchio, J. Luo, High-entropy fluorite oxides, J. Eur. Ceram. Soc. 38 (2018) 3578–3584, https://doi.org/10.1016/j.jeurceramsoc.2018.04.010.

[10] Y. Zhang, Y.J. Zhou, J.P. Lin, G.L. Chen, P.K. Liaw, Solid-solution phase formation rules for multi-component alloys, Adv. Eng. Mater. 10 (2008) 534–538, https://doi.org/10.1002/adem.200700240.

[11] N.J. Usharani, R. Shringi, H. Sanghavi, S. Subramanian, S.S. Bhattacharya, Role of size, alio-/multi-valency and non-stoichiometry in the synthesis of phase-pure high entropy oxide (Co,Cu,Mg,Na,Ni,Zn)O, Dalton Trans. 49 (2020) 7123–7132, https://doi.org/10.1039/d0dt00958j.

[12] A. Gautam, MdI. Ahmad, Stability Landscape and Charge Compensation Mechanism for Isovalent and Aliovalent Substitution in High Entropy Oxides, 2024, pp. 78–90, https://doi.org/10.1201/9781003391388-7.

[13] A. Gautam, S. Das, MdI. Ahmad, Band gap engineering through calcium addition in (Mg, Co, Ni, Cu, Zn)O high entropy oxide for efficient photocatalysis, Surf. Interfaces (2024) 104054, https://doi.org/10.1016/j.surfin.2024.104054.

[14] S.T. Murphy, H. Lu, R.W. Grimes, General relationships for isovalent cation substitution into oxides with the rocksalt structure, J. Phys. Chem. Solid. 71 (2010) 735–738, https://doi.org/10.1016/j.jpcs.2010.01.011.

[15] D. Bérardan, S. Franger, D. Dragoe, A.K. Meena, N. Dragoe, Colossal dielectric constant in high entropy oxides, Phys. Status Solidi Rapid Res. Lett. 10 (2016) 328–333, https://doi.org/10.1002/pssr.201600043.

[16] A. Salian, S. Mandal, Entropy stabilized multicomponent oxides with diverse functionality–a review, Crit. Rev. Solid State Mater. Sci. (2021), https://doi.org/10.1080/10408436.2021.1886047.

[17] A. Sarkar, R. Kruk, H. Hahn, Magnetic properties of high entropy oxides, Dalton Trans. 50 (2021) 1973–1982, https://doi.org/10.1039/d0dt04154h.

[18] S. Akrami, P. Edalati, M. Fuji, K. Edalati, High-entropy ceramics: review of principles, production and applications, Mater. Sci. Eng. R Rep. 146 (2021), https://doi.org/10.1016/j.mser.2021.100644.

[19] K. Chen, J. Ma, H. Wang, C. Li, L. An, Entropy-stabilized oxides with medium configurational entropy, Ceram. Int. 47 (2021) 9979–9983, https://doi.org/10.1016/j.ceramint.2020.12.143.

[20] G. Anand, A.P. Wynn, C.M. Handley, C.L. Freeman, Phase stability and distortion in high-entropy oxides, Acta Mater. 146 (2018) 119–125, https://doi.org/10.1016/j.actamat.2017.12.037.

[21] A.E. Danks, S.R. Hall, Z. Schnepp, The evolution of "sol-gel" chemistry as a technique for materials synthesis, Mater. Horiz. 3 (2016) 91–112, https://doi.org/10.1039/c5mh00260e.

[22] A. Varma, A.S. Mukasyan, A.S. Rogachev, K.v. Manukyan, Solution combustion synthesis of nanoscale materials, Chem. Rev. 116 (2016) 14493–14586, https://doi.org/10.1021/acs.chemrev.6b00279.

[23] A. Gautam, M.I. Ahmad, Low-temperature synthesis of five component single phase high entropy oxide, Ceram. Int. (2021), https://doi.org/10.1016/j.ceramint.2021.04.128.

[24] J. Sushil, A. Kumar, A. Gautam, M.I. Ahmad, High entropy phase evolution and fine structure of five component oxide (Mg, Co, Ni, Cu, Zn)O by citrate gel method, Mater. Chem. Phys. 259 (2021) 124014, https://doi.org/10.1016/j.matchemphys.2020.124014.

[25] J. Baek, M.D. Hossain, P. Mukherjee, J. Lee, K.T. Winther, J. Leem, Y. Jiang, W. C. Chueh, M. Bajdich, X. Zheng, Synergistic effects of mixing and strain in high entropy spinel oxides for oxygen evolution reaction, Nat. Commun. 14 (2023), https://doi.org/10.1038/s41467-023-41359-7.

[26] A. Kretschmer, D. Holec, K. Yalamanchili, H. Rudigier, M. Hans, J.M. Schneider, P. H. Mayrhofer, Strain-stabilized Al-containing high-entropy sublattice nitrides, Acta Mater. 224 (2022), https://doi.org/10.1016/j.actamat.2021.117483.

[27] B. Dubacq, A. Plunder, Controls on trace element distribution in oxides and silicates, J. Petrol. 59 (2018) 233–256, https://doi.org/10.1093/petrology/egy027.

[28] A. Amiri, R. Shahbazian-Yassar, Recent progress of high-entropy materials for energy storage and conversion, J Mater Chem A Mater 9 (2021) 782–823, https://doi.org/10.1039/d0ta09578h.

[29] J. Blundy, B.J. Wood, Prediction of crystal–melt partition coefficients from elastic moduli, Nature 372 (1994) 452–454. https://api.semanticscholar.org/CorpusID:4335750.

[30] J.C. Brice, P. Rudolph, Crystal growth, in: Ullmann's Encyclopedia of Industrial Chemistry, 2007, https://doi.org/10.1002/14356007.a08_099.pub2.

[31] J.C. Brice, Some thermodynamic aspects of the growth of strained crystals. https://api.semanticscholar.org/CorpusID:98714441, 1975.

[32] W. Hong, F. Chen, Q. Shen, Y.H. Han, W.G. Fahrenholtz, L. Zhang, Microstructural evolution and mechanical properties of (Mg,Co,Ni,Cu,Zn)O high-entropy ceramics, J. Am. Ceram. Soc. 102 (2019) 2228–2237, https://doi.org/10.1111/jace.16075.
[33] A. Kretschmer, D. Holec, K. Yalamanchili, H. Rudigier, M. Hans, J.M. Schneider, P. H. Mayrhofer, Strain-stabilized Al-containing high-entropy sublattice nitrides, Acta Mater. 224 (2022), https://doi.org/10.1016/j.actamat.2021.117483.
[34] A. Sarkar, B. Breitung, H. Hahn, High entropy oxides: the role of entropy, enthalpy and synergy, Scr. Mater. 187 (2020) 43–48, https://doi.org/10.1016/j.scriptamat.2020.05.019.